Supercapacitor Electrodes from the in Situ Reaction between Two-Dimensional Sheets of Black Phosphorus and Graphene Oxide

DOI:
10.1021/acsami.7b18853

Document Version
Accepted author manuscript

Supercapacitor electrodes from the in situ reaction between 2D sheets of black phosphorus and graphene oxide

Jianyun Cao,[†,‡] Pei He,[,†,‡] Jack R. Brent,[†] Halil Yilmaz,[†] David J. Lewis,[†] Ian A. Kinloch,[†] and Brian Derby*[,†]*

[†]School of Materials, University of Manchester, Oxford Road, Manchester M13 9PL, U.K.

[‡]These authors contributed equally

Email: pei.he@manchester.ac.uk; brian.derby@manchester.ac.uk

KEYWORDS: *graphene oxide, black phosphorus, degradation, liquid electrolyte, supercapacitors*

ABSTRACT

2D materials show considerable promise as high surface area electrodes for energy storage applications such as supercapacitors. A single sheet of graphene possesses a large specific surface area due to its atomically thin thickness. However, in order to package this area efficiently in a device, it must be confined within a finite 3D volume without restacking of the sheet faces. Herein we present a method of maintaining the high surface area through the use of a hybrid thin film in which few-layer exfoliated black phosphorus (BP) reduces graphene oxide (GO) flakes. When the film is exposed to moisture, a redox reaction between the BP and the GO forms an interpenetrating network of reduced graphene oxide (RGO) and a liquid electrolyte of intermediate phosphorus acids H_xPO_y. The presence of the liquid H_xPO_y electrolyte in the RGO/H_xPO_y film stabilizes and preserves an open channel structure enabling rapid ion diffusion, leading to an excellent charging rate capability (up to 500 mV s^{-1}, and retaining 62.3% of initial capacitance at a large current density of 50 A g^{-1}) when used as electrodes in supercapacitors.

INTRODUCTION

Graphene oxide (GO) is a single layer graphene sheet functionalized with oxygen groups, various macroscale structures can be fabricated by using GO sheets as basic building blocks, such as film, paper, fiber, hydrogel, aerogel, etc.[1-3] Reduction of GO leads to reduced graphene oxide (RGO) with much greater electrical conductivity.[4-5] Graphene films, assembled from overlapping RGO sheets, show high electrical conductivity (~7200 S m^{-1}) and good mechanical strength (150 MPa in tension),[6-7] and have been widely studied as electrode materials for electrochemical supercapacitors.[8-11] However, during film deposition and drying, compact face-on-face restacking of graphene sheets may occur. This both reduces the surface area and limits the rapid transport of electrolyte ions into the inner structure of the graphene film, leading to a reduction in electrochemical performance, particularly rate capability.[10] Restacking of graphene sheets is typically prevented by inserting spacers between the graphene sheets, e.g. metal or metal oxide nanoparticles, carbon nanotubes and carbon black.[12-14] Another approach to prevent graphene restacking is to use the principles of colloid chemistry to maintain a stable liquid phase between the graphene layers.[10-11] The colloidal approach has been demonstrated with chemically modified or reduced graphene oxide (RGO) where non-planar sheets of graphene containing oxygen defects interact with the surrounding solvent molecules preventing face-face contact. Even after the removal of the majority of the solvent phase, a hybrid material of non-planar graphene sheets separated by stable, nanometer thick, bound solvent layers has been reported.[10] Further study has demonstrated that by using a mixture of two liquids (e.g. water in sulfuric acid solution), a liquid electrolyte (in this case sulfuric acid) can be retained inside the graphene film.[11] This not only prevents restacking of the graphene sheets in an electrode but also provides the electrolyte required for charging and discharging a supercapacitor, leading to improved rate capability.

2D Black phosphorus (BP) has attracted considerable interests from the research community due to its extraordinary electrical and optoelectronic properties.[15-19] However, it is well established that mono- or few-layer BP, produced by both mechanical exfoliation and solution phase exfoliation, is unstable and degrades in the presence of oxygen and water under ambient conditions,[20-23] to form phosphorus acids. However, despite extensive experimental and theoretical studies,[22-26] the detailed mechanisms of the degradation of BP remain unconfirmed, as are the precise degradation products. Recent studies have shown that this reaction finally forms phosphorus containing acids, such as phosphorous acid (H_3PO_3),[22] phosphoric acid (H_3PO_4),[23-24] or a mixture of H_3PO_3 and H_3PO_4,[25] while the intermediate compounds might contain hypophosphorous acid (H_3PO_2).[25] Previous research has shown that hypophosphorous acid is capable of reducing graphene oxide (GO), with the as-reduced GO film exhibiting an electrical conductivity of 380 S m^{-1}.[27] Here we report on a combination of GO with BP into a hybrid material (GO/BP), in which the BP acts both as a spacer to prevent the stacking of GO sheets and also, as a reducing agent in the presence of H_2O, to chemically modify the GO to RGO sheets. A product of the interaction of H_2O with BP is a complex solution of phosphorous containing acids (H_xPO_y),[22, 24-25] it is hypothesized that this will produce an electrolyte that may be capable of stabilizing the RGO sheets through colloidal processes to prevent their stacking.[10-11] The as-formed RGO film stabilized by H_xPO_y electrolyte (RGO/H_xPO_y) has been studied as electrode materials for supercapacitors in this work.

EXPERIMENTAL SECTION

Preparation of GO/BP hybrid film: BP crystal was purchased from Smart Elements (Vienna, Austria). Natural graphite flakes (Grade 9842) were purchased from Graphexel Ltd., (Epping,

UK). Concentrated H_2SO_4 (>17.7 mol) was purchased from Fisher Scientific (Loughborough, UK). All other chemicals were purchased form Sigma-Aldrich (Gillingham, Dorset, UK). Few layer BP flakes were prepared by liquid phase exfoliation.[15] GO flakes were prepared by the modified Hummers' method.[28] The GO/BP hybrid film was prepared by vacuum filtration of a mixed dispersion of GO and BP flakes. Briefly, 0.22 mL of concentrated GO dispersion (3.5 mg mL^{-1}) in absolute ethanol was mixed with 2 mL BP flakes dispersion in acetonitrile (0.2 mg mL^{-1}). After mixing, the mixture was diluted with acetonitrile to a total volume of 30 mL. The mass ratio of GO to BP is 2 to 1. The mixed dispersion was subjected to bath sonication for 30 min and the solvent removed by vacuum filtration with a PTFE filter membrane (Omnipore, 0.1 μm pore size, 25 mm diameter). After filtration, the GO/BP hybrid film was peeled from the filter membrane in absolute ethanol and used in further experiments.

Preparation of RGO/H_xPO_y film: Transformation of the GO/BP hybrid film to a RGO/H_xPO_y film was achieved by exposing the GO/BP hybrid film to 100% humidity at 25 °C for 120 h. The 100% humidity environment was achieved inside an enclosed VWB 18 water bath chamber (VWR, Soulbury, UK) with one third of its volume filled with de-ionized water at 25 °C, and the GO/BP hybrid film placed in the humid atmosphere above the water level. The humidity level was monitored with a commercial humidity sensor (ST-321 Humidity Meter: Farnell Element 14, Leeds UK). Finally, the as-formed RGO/H_xPO_y film was put into the vacuum oven (Fistreem, Loughborough, UK) with a vacuum of ~13 mbar at room temperature to evaporate the absorbed water. For a control specimen, a pure RGO film was prepared by soaking the RGO/H_xPO_y film in de-ionized water to remove the as-formed H_xPO_y acids. This RGO film was also vacuum treated, following the same procedure as the RGO/H_xPO_y film, to remove any water trapped between the RGO layers.

Material and film characterization: The morphology of the GO sheets was characterized by a Dimension 3100 atomic force microscope (AFM) (Bruker, Bilericca, MA, USA) using tapping-mode imaging. Scanning electron microscope (SEM) images and enery dispersive X-ray elemental analyses (EDX) were obtained using a Zeiss Sigma VP field emission SEM (Carl Zeiss, Jena, Germany). Transmission electron microscopy (TEM) characterization was conducted with a CM20 TEM (FEI, Eindhoven, Netherlands). X-ray diffraction (XRD) characterization was conducted with a X'Pert Pro X'Celerator diffractometer (PANalytical: Almelo, Netherlands). Raman spectroscopy was performed on a Renishaw 1000 spectrometer with an excitation laser wavelength of 633 nm, curve fitting was conducted by Wire 4.1 software with Lorentz functions. Fourier transform infrared spectrum (FT-IR) was measured with a Nicolet 5700 spectrometer (Thermo Fisher Scientific, Waltham. MA, USA). X-ray photoelectron spectroscopy (XPS) was performed with a Kratos Axis Ultra X-ray photoelectron spectrometer meter (Kratos, Manchester, UK); curve fitting was accomplished by CasaXPS software. Contact angle measurement was carried out by a Krüss Drop Shape Analyzer DSA100 (Krüss, Hamburg, Germany). The sheet resistance of RGO film was measured using a Jandel four-probe station (Jandel Engineering, Linslade, UK) equipped with a Keithley 2182A nanovoltmeter and a Keithley 6220 current source (Keithley Tektronix, Beaverton, USA), .

Fabrication of supercapacitors based on RGO/H_xPO_y film: Supercapacitor based on RGO/H_xPO_y film was assembled by two pieces of RGO/H_xPO_y film with a piece of PTFE filter membrane (Omnipore, 0.2 μm pore size) as separator. Prior to assembly, the RGO/H_xPO_y films and PTFE filter membrane were soaked in 1 M H_3PO_4 overnight. As control experiment, supercapacitor was also fabricated by the RGO film which the as-formed

H_xPO_y acids electrolyte has been washed away. All electrochemical experiments were carried out using an electrochemical workstation, Ivium Stat (Ivium Technologies, Eindhoven, Netherlands). The specific capacitance (C) of the materials (F g^{-1}) based on galvanostatic discharge is calculated as follows [29-30]:

$$C = \frac{I\Delta t}{m\Delta V} \tag{1}$$

$$C = 4C_{cell} \tag{2}$$

where C_{cell} is the capacitance per total mass of the two electrodes in the cell (F g^{-1}), I is the discharge current (A), Δt is the discharge time (s), ΔV is the operating potential/cell voltage range excluding the IR drop (V), m is the total mass of active materials in the two electrodes.

The energy density of the supercapacitor was calculated as follows [29]:

$$E = \frac{1}{2}C_{cell}V^2 \tag{3}$$

$$P = \frac{E}{\Delta t} \tag{4}$$

Where E is the energy density (Wh kg^{-1}), V is the working cell voltage (V), P is the power density (W kg^{-1}).

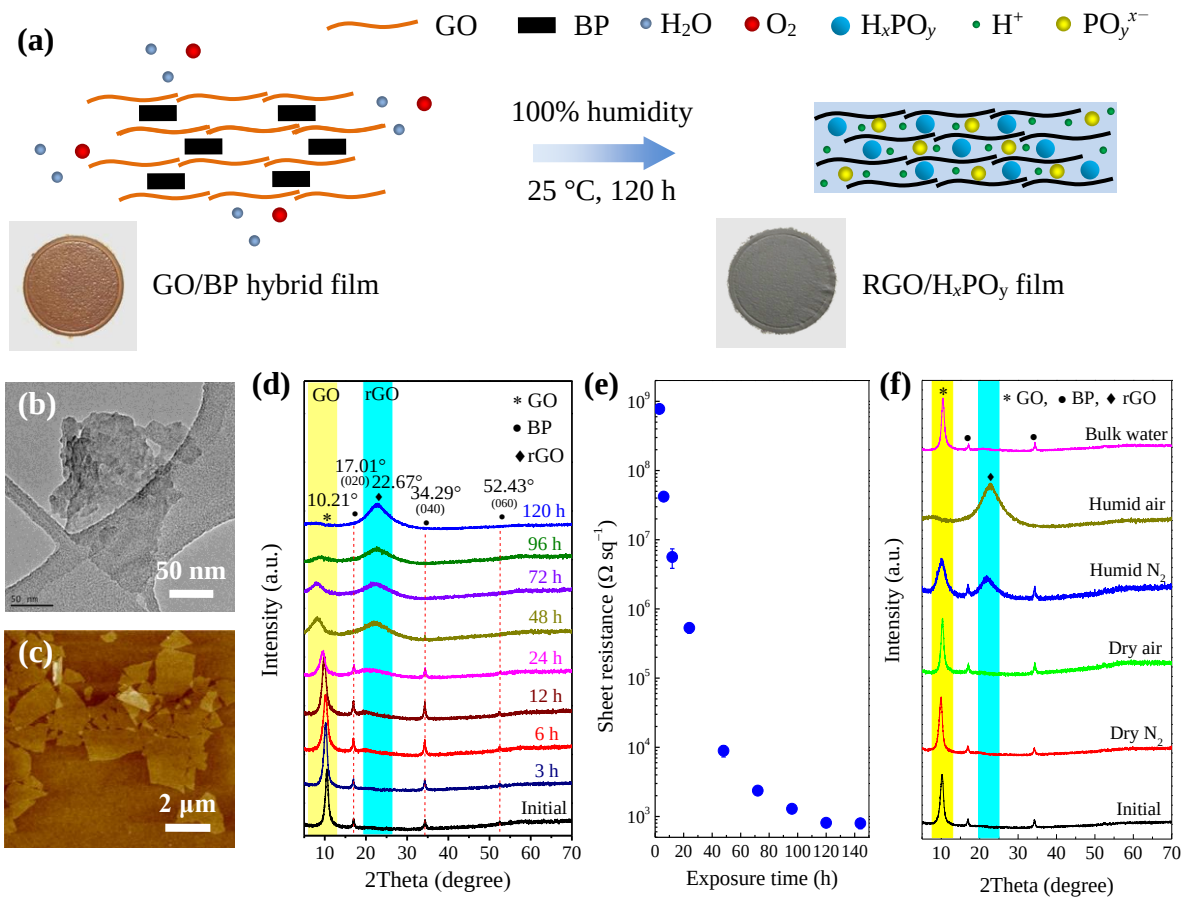

Figure 1. (a) Schematic illustration of the *in situ* reduction of GO by BP and formation of H_xPO_y electrolyte, the left and right photographs show the initial GO/BP hybrid film and the as-formed RGO/H_xPO_y film, respectively. (b) TEM image of liquid phase exfoliated few layer BP flakes. (c) AFM image of GO sheets. (d) Evolution of the XRD pattern obtained from the GO/BP hybrid film with increasing time of exposure to 100% humidity at 25 °C. (e) Evolution of the sheet resistance of the GO/BP hybrid film with increasing time of exposure to 100% humidity at 25 °C. (f) XRD patterns of the GO/BP hybrid film after being exposed to a range of environments at 25 °C for 120 h.

RESULTS AND DISSCUSSION

Hybrid films of GO and BP were prepared by the vacuum filtration of a mixed dispersion of nanosheets of the materials. Figure 1a shows a schematic illustration of the proposed transformation of the GO/BP hybrid film to a RGO/H_xPO_y film through a redox reaction between the BP and GO. This is accompanied by a change in colour of the GO/BP hybrid film from brown to black. Figure 1b shows a typical TEM image of the BP flakes produced by the liquid exfoliation method, reported earlier by Brent et al.[15] The as-exfoliated BP has an average size of 72 ± 30 nm, with most flakes being 50~100 nm in diameter (see Figure S1 for other TEM images of BP flakes and the flake size distribution). According to the AFM characterization (Figure S2), the thicknesses of the exfoliated BP flakes are generally below 6 nm, with a mean thickness of 3.3 ± 1.2 nm, suggesting the flakes are predominantly 3 layers.[15] Figure 1c shows a typical AFM image of GO flakes, further analysis found a mean lateral diameter of 1.33 ± 0.45 μm with the majority of the flakes were in the size range 1~2 μm (Figure S3c). Height profile of a GO flake is show in Figure S3b, suggesting a thickness of ~ 1 nm. Statistically analyzing 100 GO flakes (see Figure S3d for the thickness distribution) lead to a mean thickness of 1.04 ± 0.1 nm, and all flakes are below 1.5 nm in thickness, indicating the GO flakes are predominantly single layer.

Figure 1d shows a sequence of XRD patterns taken from the hybrid film after exposure to air at 100% relative humidity for periods of up to 120 h. The diffraction peaks from the initial GO/BP hybrid film at 17.01°, 34.29° and 52.43°, are assigned to BP reflections from (020), (040) and (060) planes respectively; a strong GO peak is also visible at 10.21° (see Supporting Information Figure S4 for the XRD pattern from a pure BP crystal). As the time of exposure to the humid environment increases, the intensity of the BP and GO reflections decreases. Interestingly, the GO peak reflection angle (2θ) decreases from 10.21° to 8.24°

after 24 h exposure, suggesting that the GO sheets are swelling due to the intercalation of water molecules.[31] After 24 h exposure, there is a considerable reduction in the intensity of the BP peaks and the emergence of a peak at $2\theta = 22.67°$, which is assigned to RGO.[6] The diffraction peaks for BP disappear after 48 h exposure, however, the reduction in the GO peak and a parallel increase in the RGO peak continue beyond this time before reaching equilibrium after about 120 h. We interpret that the continued reduction of the GO reflection angle as its intensity decreases indicates the continued swelling of the GO galleries, allowing gradual access of the H_xPO_y produced by the degradation of BP to an increasing large area of the GO. When reduction of the GO commences, it reduces the H_xPO_y concentration of the electrolyte, driving further degradation of the BP. Once all the BP has been consumed, reduction of the GO to RGO can continue until the H_3PO_2 content of the electrolyte is consumed or the GO has been fully reduced, thus explaining the continuing change in the GO and RGO peak intensities after the disappearance of the BP diffraction peaks.

Further evidence for the reduction of GO is provided by monitoring the evolution of the sheet resistance of the GO/BP hybrid film with increasing time of exposure to 100% humidity air (Figure 1e). The sheet resistance of the GO/BP hybrid film drops monotonically by six orders of magnitude with increasing exposure time. After 120 h, the sheet resistance of the as-formed RGO/H_xPO_y film is $796 \pm 92\ \Omega\ sq^{-1}$, corresponding to an electrical conductivity of $837 \pm 98\ S\ m^{-1}$ (film thickness of ~ 1.5 μm).

To further investigate the role of O_2 and H_2O in the transformation of the GO/BP hybrid film, XRD patterns were obtained from the GO/BP films after 120 h exposure to various environments and conditions, as shown in Figure 1f. There is almost no visible change in the relative intensity of the peaks in the XRD pattern, when compared with the as-received state,

after the GO/BP hybrid film is exposed to dry N_2 or dry air. However, exposure of the GO/BP film to 100% humid N_2 leads to the weakening of peaks corresponding to GO and BP and the appearance of a new broad peak corresponding to RGO. These results suggest that the presence of H_2O dominates the BP degradation mechanism and assists the reduction of GO. The change after exposure to humid N_2 is less marked that that seen after exposure to humid air, indicating that the presence of O_2 accelerates this process. The degradation of BP in the presence of water but without oxygen is consistent with previous observations and predictions.[17] Note that the XRD pattern obtained from a GO/BP hybrid film immersed in liquid water shows the degradation of BP, but with no apparent change to the GO peak. This is likely to be the result of the excess water diluting the H_xPO_y electrolyte diminishing its effectiveness in reducing the GO. Table S1 in the supplementary information summarizes the extent of transformation of the GO/BP hybrid films under various environments.

Raman spectroscopy was also used to track the reduction of GO in this work, 5 spectra were recorded from each sample at random locations, the recorded spectra were fitted by Lorentz functions at a range of 1000 to 2000 cm^{-1}, thus the intensity (I) and full width at half-maximum (FWHM, plotted as Γ) of G and D bands can be analyzed, see Figure S5a for the examples of fitted spectra for the initial GO/BP film and the film with 72 h of exposure. Based on previous reports,[32] GO prepared using Hummer's method are highly defective, thus no significant change in the Raman spectra is expected after reduction. Consistent with this, Raman spectra from the GO/BP hybrid film after various times of exposure to 100% humidity (Figure 2a) all exhibit similar features with broad D and G bands, and the I_D/I_G ratio showing no significant difference (Figure S5b).

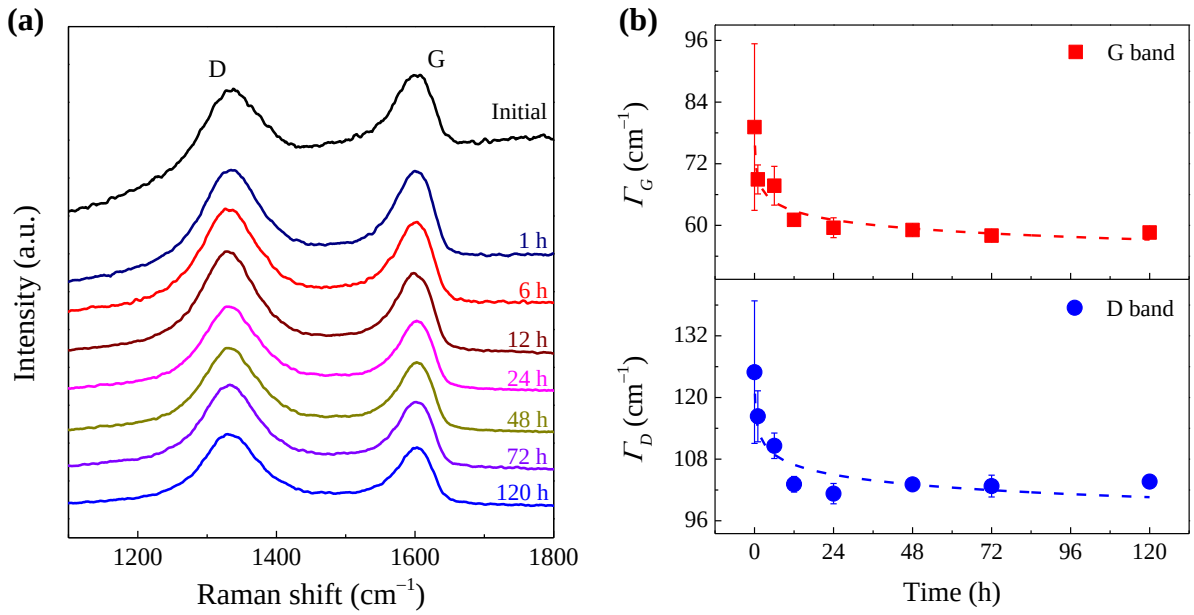

Figure 2. (a) Typical Raman spectra obtained from the GO/BP hybrid film being exposed to 100% humidity at 25 °C for various times; (b) Evolution of FWHM of the G and D bands with increasing time of exposure to 100% humidity.

Nevertheless, by analyzing the fitted results, we found that the average FWHM for the G and D bands decrease quickly in the first 24 h of exposure, and then remain stable at ~ 60 cm^{-1} for the G band and ~104 cm^{-1} for the D band (Figure 2b). The decrease of Γ_G in the first 24 h could be related to the reduction of GO according to the previous investigation.[33] The small change in Γ_G after 24 h suggests that the reduction of GO is probably completed within the first 24 h. However, this assumption is in conflict with the XRD results, which indicates the complete reduction of GO requires up to 96 h. Considering the diffusion of water and oxygen molecules starts from the surface of the GO/BP hybrid film, hence the reduction reaction will occurs firstly near the surface. On the other hand, the analyzing depth of Raman spectroscopy is limited by the transmittance of the sample to the laser used, thus RGO with black colour will limit the sensitivity of Raman spectroscopy to the few layers of RGO near surface. Hence, it is reasonable to suppose that the reduction of GO layers located near the surface can

be finished in the first 24 h, but for the GO in the bulk film, thorough reduction requires up to 96 h based on the XRD results. For the control samples, representative Raman spectra are displayed in Figure S6, and the corresponding comparison of Γ_D, Γ_G and I_D/I_G ratio is available in Figure S6 b, c and d, respectively. The results suggest that the Γ_G values for GO/BP films exposed to humid air and N_2 for 72 h show obvious decrease due to GO reduction when compared with that in dry air and bulk H_2O. These results are consistent with the XRD characterization shown in Figure 1.

FT-IR spectra further confirmed the reduction of GO and the formation of phosphorus containing acids. As shown in Figure 3a, the characteristic peaks of oxygen functionalities appear in the spectrum of the GO/BP hybrid film, including: the stretching vibration peak of C=O at 1735 cm^{-1}, the O−H peak at 1409 cm^{-1} and the C−O epoxide peak at 1233 cm^{-1}.[34] In contrast, the RGO/H_xPO_y film exhibits a clear peak at 1580 cm^{-1}, corresponding to the C=C stretching band,[34] and a weak C=O peak at 1735 cm^{-1}, again suggesting the removal of most of the oxygen functionalities. The presence of phosphorus acids is seen with the peak located at 1227 cm^{-1}, (P=O stretching) and the peak at 1038 cm^{-1} (P-OH bending).[35] For comparison, the FT-IR spectra of control samples (stored in various environments and conditions for 72 h) were also recorded (see Figure S7). Reduction of GO only occurred with the GO/BP film stored in the humid N_2, and no obvious change in the characteristics of FT-IR spectra recorded from the GO/BP films stored in dry air, dry N_2 and vacuum. The FT-IR results are consistent with those of the XRD and Raman characterization.

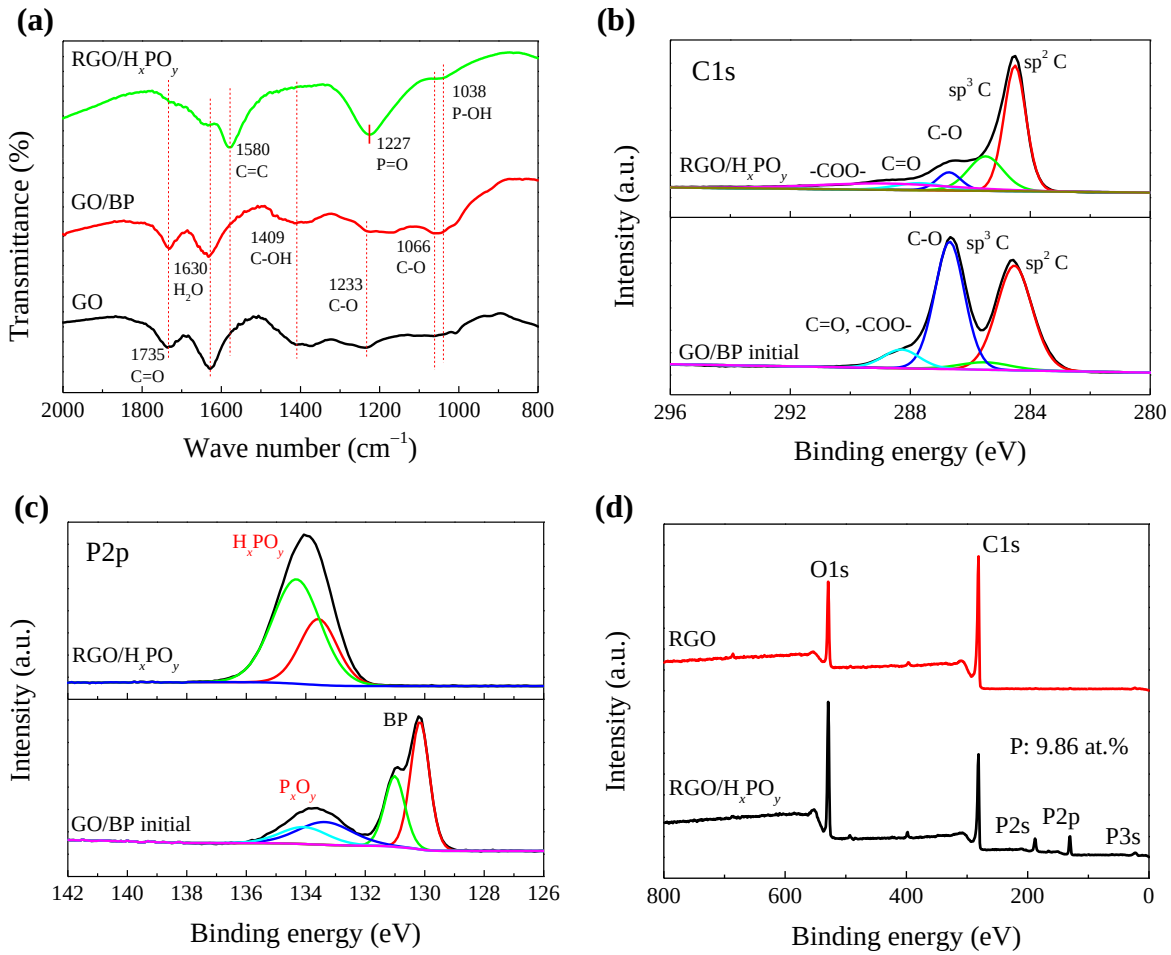

Figure 3. (a) XPS C1s spectra of GO and RGO/H_xPO_y film. (b) XPS P2p spectrum of RGO/H_xPO_y film. (c) XPS survey spectra of RGO/H_xPO_y and RGO (prepared by washing RGO/H_xPO_y film with water to remove H_xPO_y acids. (d) FT-IR spectra of GO, initial GO/BP hybrid film, and RGO/H_xPO_y films.

The structural changes in the GO/BP hybrid film exposed to humid air were further investigated using XPS. Figure 3a compares the C1s spectra from the initial GO/BP hybrid film and the RGO/H_xPO_y film. This shows that the majority of the oxygen functionalities on the GO sheets have been reduced. Figure 3b compares the high-resolution P2p spectra of the initial GO/BP hybrid film and the RGO/H_xPO_y film formed after exposure to humidity. The majority of the phosphorus in the initial GO/BP hybrid film exists as pristine BP, confirmed by the $P2p^{1/2}$ component at 131.0 eV and $P2p^{3/2}$ component at 130.1 eV. Components

corresponding to the oxidized phosphorus (PO_x) also exist, probably due to the partial degradation that occurs during the solution exfoliation and the vacuum filtration process.[17, 36] After being exposed to 100% humidity for 120 h, the BP degraded totally and a single peak related to oxidized phosphorus is present. Since phosphorus oxides tend to hydrolyze in humid atmospheres, the most likely state of these phosphorus oxides is liquid acids (H_xPO_y). An XPS survey spectrum of the RGO/H_xPO_y film (Figure 3c) suggests that the film contains 9.86 at.% P. The as-formed H_xPO_y acids can be easily washed away by soaking the RGO/H_xPO_y film in water overnight, as confirmed by the XPS survey spectrum of the as-formed RGO film shown in the supplementary information (Figure S8). The oxygen contents of the RGO/H_xPO_y and RGO film are measured as 28.05 at.% and 16.21 at.%, respectively, suggesting that nearly half of the oxygen in the RGO/H_xPO_y film is bound to the phosphorus. These as-formed acids are believed to be trapped between the RGO layers. The structure of the RGO/H_xPO_y film is similar to that previously reported with other liquid mediated graphene films.[11] It is proposed that the acid electrolyte within the RGO layers interacts with and prevents the graphene sheets from closely restacking and serves as an electrolyte enhancing the electrochemical performance.

SEM was used to image and characterize the surface morphologies of the initial GO/BP hybrid film (Figure 4a), the as-formed RGO/H_xPO_y film (Figure 4b), and the washed pure RGO film (Figure 4c). These films show distinct differences; the initial GO/BP hybrid film has a surface with a particulate morphology, due to the presence of BP nano-flakes amongst the larger GO sheets. In contrast, after exposure to humid air, the as-formed RGO/H_xPO_y film shows a smooth surface, confirming the degradation and elimination of the BP flakes to form a liquid acid electrolyte. Note that the RGO/H_xPO_y film was vacuum treated at ~13 mbar overnight to remove the volatile water, leaving nonvolatile concentrated H_xPO_y liquid acid

trapped between the graphene layers inside the film. The surface of the washed RGO film shows a wrinkled morphology typical of graphene films, which is distinct from the RGO/H_xPO_y film. The reason for the appearance of micro-wrinkles is related to the complete removal of the nonvolatile liquid acids by washing. After washing, the liquid acids are exchanged by water, and the capillary force generated during the subsequent vacuum evaporation of water and the restacking of the RGO sheets generates the micro-wrinkles.[10] Mass ratios of C, O and P elements present in the films were determined by EDX mapping (Supporting Information Figure S9) with the mass ratio of P measured as 10.2 wt.% in the RGO/H_xPO_y film, but only 0.4 wt.% P in the washed pure RGO film, which is consistent with the XPS results.

SEM cross sections and the corresponding EDX composition maps of the RGO/H_xPO_y film and washed RGO film are shown in Figure 4d and e. The thickness of the as-formed RGO/H_xPO_y film is around 1.5 µm, and the phosphorus is homogeneously distributed throughout the film. Once the as-formed H_xPO_y acids have been washed away, the washed pure RGO film shows a reduced thickness of about 1 µm (Figure 4e), and a much weaker phosphorus signal was detected by EDX. The hydrophilicity of the as-formed RGO/H_xPO_y film and the washed pure RGO film was determined by measuring the water contact angle. As shown in Figure 4f and g, the water contact angle for RGO/H_xPO_y film and the washed RGO film is 65.6° and 84.6°, respectively, suggesting better hydrophilicity of the RGO/H_xPO_y film due to the existence of water miscible H_xPO_y acids.

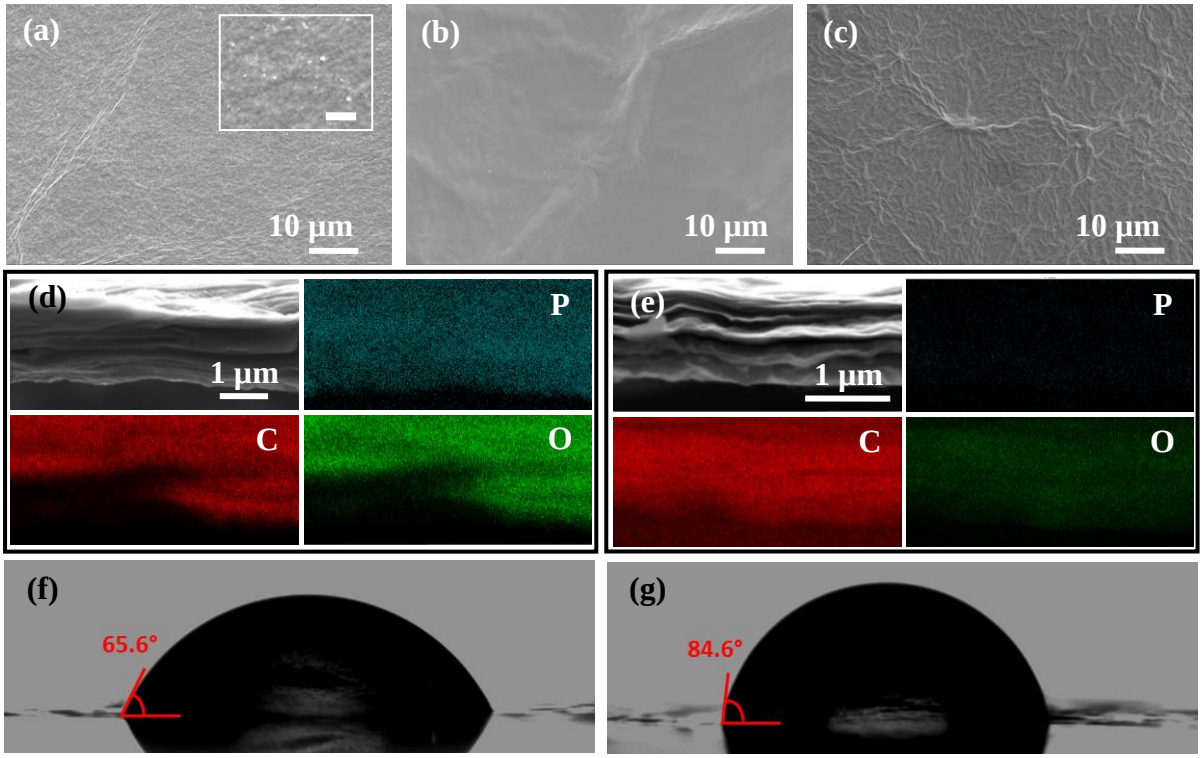

Figure 4. SEM surface morphology of (a) initial GO/BP hybrid film (scale bar in the inset: 2 μm), (b) RGO/H_xPO_y film and (c) washed pure RGO film. SEM cross-section morphologies of (d) RGO/H_xPO_y film and (e) washed RGO film, as well as the corresponding EDS mapping of P, C and O elements. Water contact angels for (f) RGO/H_xPO_y and (g) washed RGO films

Based on these results, we hypothesize a possible reaction mechanism for the transformation of the GO/BP hybrid film, in which BP is degraded *via* reaction with H_2O and O_2, these degradation products subsequently reduce the GO to form conductive RGO. The FT-IR data (Supporting Information Figure S10) shows the degradation products of the BP has similar peaks to those found with H_3PO_2, H_3PO_3, and H_3PO_4 but is not exactly the same as any of them, indicating that the degradation products are likely to be a mixure of phosphorus oxyacids, which is consistent with previous findings.[22, 25] The XRD spectra obtained from GO films immersed in H_3PO_2, H_3PO_3, and H_3PO_4 are compared in Figure S11. The peak corresponding to GO disappears and an RGO peak appears for the film immersed in H_3PO_2,

while the GO films immersed in H_3PO_3 and H_3PO_4 show no noticable changes to their XRD spectra. This obersvation confirms that only H_3PO_2 in the H_xPO_y reaction product from the interaction of BP with humid atmospheres is capable of reducing GO to RGO.

Hence, we propose that the degradation of BP results in the formation of H_3PO_2 by:

$$4P + O_2 + 6H_2O \rightarrow 4H_3PO_2 \quad (5)$$

Other oxyacids of phosphorus may also form but onle H_3PO_2 can further react with and reduces GO leading to the formation of H_3PO_3 or H_3PO_4.[27] This is indicated schematically in Figure 5 in accordance with previous reports on the reduciton of GO by hydroxylamine and $NaHSO_3$.[37-38] The nucleophilic attack results in ring opening of the epoxide groups followed by proton transfer, with the elimination of water leading to the formation of an unstable intermediate, which further converts to a conjugated vinyl and phosphorus acid *via* reaction with water.

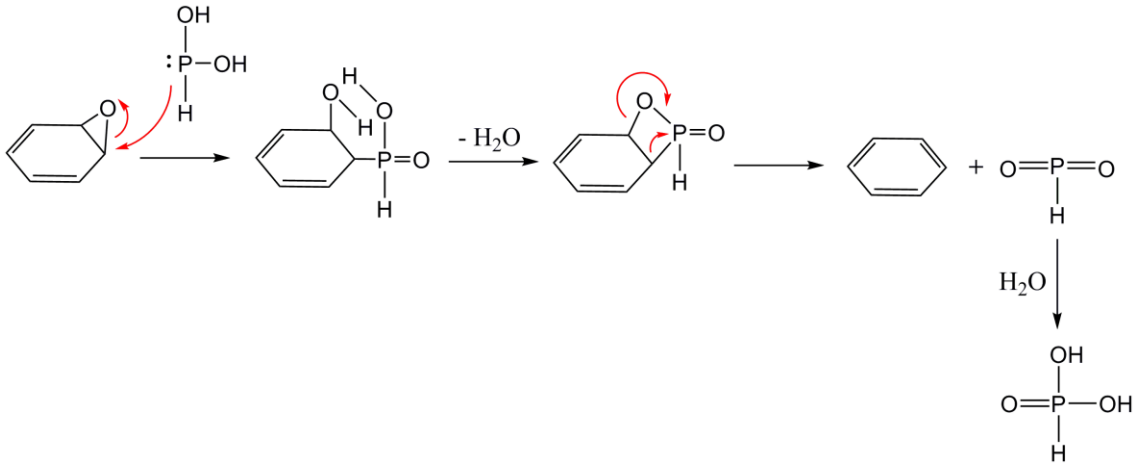

Figure 5. Possible mechanism for the reduction of GO by H_3PO_2.

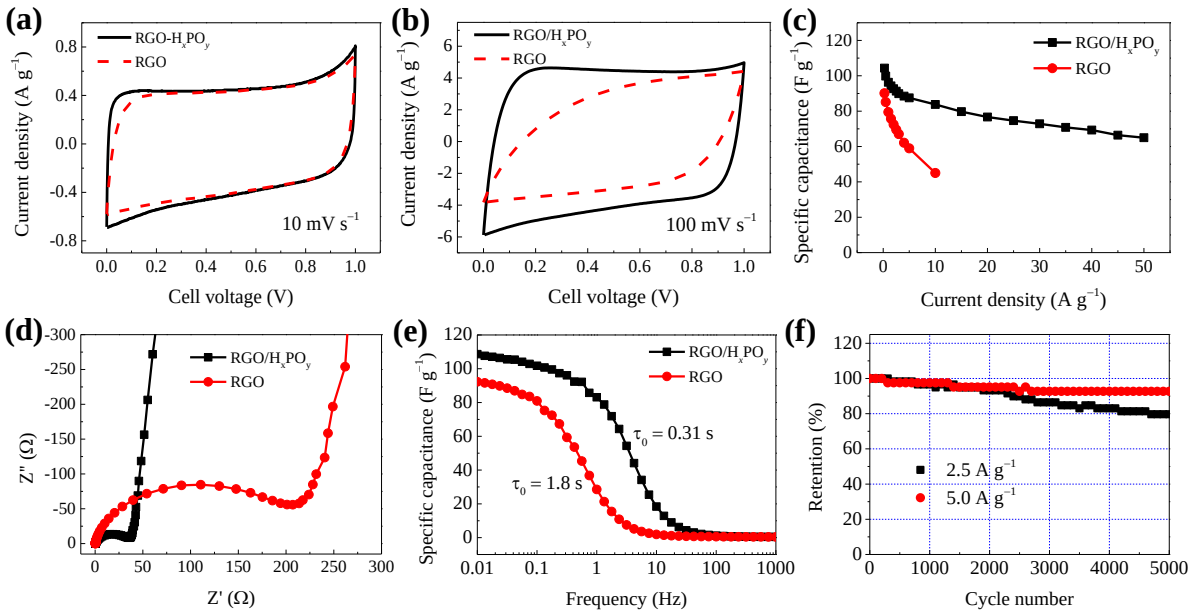

Figure 6. Electrochemical performance of supercapacitor based on RGO/H_xPO_y film. Comparison of CV curves of supercapacitors based on RGO/H_xPO_y and washed RGO films at (a) 10 and (b) 100 mV s^{-1}. (c) Rate capabilities of supercapacitor based on RGO/H_xPO_y and washed RGO films. (d) Nyquist plots for the supercapacitors based on RGO/H_xPO_y and washed RGO films. (e) Evolution of specific capacitances with frequency for the RGO/H_xPO_y and washed RGO films. (f) Cycling stability of the supercapacitor based on RGO/H_xPO_y film.

To investigate the applicability of the RGO/H_xPO_y film, we fabricated a symmetric supercapacitor using two pieces of the RGO/H_xPO_y film as electrodes and 1 M H_3PO_4 aqueous solution as the electrolyte. For comparison, a supercapacitor based on a washed pure RGO film was also fabricated. Figure 6a and b compare the cyclic voltammetry (CV) curves of the RGO/H_xPO_y and RGO supercapacitors at scan rates of 10 and 100 mV s^{-1}, respectively. At the slow scan rate of 10 mV s^{-1}, both the CV curves of RGO/H_xPO_y and RGO supercapacitors show a good rectangular shape, indicating that the ion transport inside the graphene film is not inhibited. However, at a higher scan rate of 100 mV s^{-1}, the CV

curve of the hybrid RGO/H_xPO_y supercapacitor still maintains the desired rectangular characteristic while that of the RGO supercapacitor deteriorates markedly from the ideal. This phenomenon suggests a sluggish transport of electrolyte ions in the densely restacked RGO film, while in the RGO/H_xPO_y film, the channels for ion diffusion are preserved by the presence of H_xPO_y acids, leading to an excellent rate capability. A similar behavior and mechanism for enhanced ionic conductivity has been reported by Yang et al. who presented similar electrode behavior with RGO electrodes produced by the reduction of GO by N2H4 and stabilized by colloidal dispersion.[10, 11] Detailed comparison of the CV curves at various scan rates ranging from 20 to 500 mV s^{-1} is available in the supplementary information (Supporting Information Figure S12). The rectangular characteristics of the CV curves for the RGO/H_xPO_y film at high scan rates are approaching that of a liquid electrolyte-mediated graphene film.[11]

Galvanostatic charge-discharge experiments were used to further evaluate the rate performance of the RGO/H_xPO_y supercapacitor (Supporting information Figure S13). Figure 6c shows that the RGO/H_xPO_y film exhibits higher specific capacitance at all discharging rates compared with the RGO film, especially at large current densities. At a small discharge current density of 0.25 A g^{-1}, the RGO/H_xPO_y film had a specific capacitance of 104.4 F g^{-1}, higher than that of the RGO film (90.1 F g^{-1}). The higher specific capacitance of RGO/H_xPO_y film is believed to be due to the H_xPO_y acids trapped between the graphene layers, which prevent the graphene from restacking through colloidal stabilization mechanisms. Moreover, the RGO/H_xPO_y film maintains a high specific capacitance (65.0 F g^{-1}) even at a large current density of 50 A g^{-1}, while the specific capacitance of the RGO films drops rapidly with a specific capacitance of 45 F g^{-1} at a current density of 10 A g^{-1}. The specific capacitance of RGO/H_xPO_y film (104.4 F g^{-1} at 0.25 A g^{-1} and 65.0 F g^{-1} at 50 A g^{-1}) is better than that of

the previously reported macro-porous graphene film (58.1 F g^{-1} at 1 A g^{-1}),[39] electrochemically exfoliated graphene (56.6 F g^{-1} at 1 mV s^{-1}),[40] GO reduced by Zn powder (68 F g^{-1} at 5 A g^{-1}),[41] electrophoretic deposited graphene on carbon cloth (70 F g^{-1} at 1 A g^{-1})[42] and RGO/carbon black hybrid gel film (95.7 F g^{-1} at 5 mV s^{-1}).[13] The specific capacitances of RGO/H_xPO_y film are also comparable with the graphene-cellulose paper (120 F g^{-1} at 1 mV s^{-1}),[43] pristine graphene aerogel (123 F g^{-1} at 1 A g^{-1}),[44] and the liquid electrolyte mediated graphene film (100 F g^{-1} at 100 A g^{-1}).[11] See Table S2 in the supplementary information for a more detailed comparison of this data.

Electrochemical impedance spectroscopy (EIS) was also performed to investigate the role of the as-transformed H_xPO_y acid electrolyte. As shown in Figure 6d, the internal resistance of the RGO supercapacitor, determined by the high frequency intercept along the *x*-axis, is much larger than that of the RGO/H_xPO_y supercapacitor. Figure 6e shows plots of specific capacitance versus frequency for the RGO/H_xPO_y and RGO supercapacitors. At low frequency, the specific capacitance of the RGO/H_xPO_y supercapacitor is larger than that made with RGO, which is consistent with the galvanostatic discharging results. Moreover, the relaxation time of the supercapacitor, determined by frequency at half of the initial capacitance, is 0.31 s for the RGO/H_xPO_y supercapacitor, which is much shorter than that for the RGO (1.8 s), corresponding to an enhanced rate capability. Ragone plots (energy density versus power density) of the supercapacitors based on the RGO/H_xPO_y film and the washed RGO film are available in Figure S14 in the supporting information. The RGO/H_xPO_y film is able to maintain an energy density of 2.2 Wh kg^{-1} at a high power density of 48 kW kg^{-1}. The relative low energy density of RGO/H_xPO_y film when compared to the commercial supercapacitor based on activated carbon (~5 Wh kg^{-1}) is due to the use of an aqueous electrolyte, which limits the cell voltage to 1.0 V. Finally, the cycling stability of the

RGO/H_xPO_y film was investigated by galvanostatic charging-discharging at current densities of 2.5 and 5 A g^{-1}. As shown in Figure 6f, the supercapacitor based on RGO/H_xPO_y film is able to be charged and discharged for 5000 cycles with retention of 92.7% at 5 A g^{-1} and 79.6% at 2.5 A g^{-1}. We note that similar highly stable supercapacitor performance after repeated cycling has been reported by Yang et al using colloidally stabilized RGO sheets.[10,11] In our case we have proposed that the H_xPO_y acids present in the electrolyte act as colloidal stabilisers, preventing the restacking of RGO sheets, thus the mechanisms for the long term stability of the electrodes are probably similar to those occurring in Yang et al's experiments. Further study is needed to determine the mechanisms for the cycling stability of the electrodes and performance after longer times.

We further investigated the effect of GO to BP mass ratio in the initial hybrid film on the electrochemical performance of the as-formed RGO/H_xPO_y film. As shown in Figure 7a and b, by increasing the content of BP in the initial hybrid film from GO:BP = 2:1 to GO:BP = 1:2, the CV curves of the as-derived RGO/H_xPO_y film at both 10 and 100 mV s^{-1} show slightly larger enclosed area. According to the rate capability (Figure 7c), the specific capacitance of the RGO/H_xPO_y film with an initial GO:BP ratio of 1:2 shows slightly higher specific capacitance at all current density range than that of the film with an initial GO :BP ratio of 2:1. In addition, the RGO/H_xPO_y film with an initial GO:BP ratio of 1:2 shows smaller internal resistance in the Nyquist plots (Figure 7d) than that of the film with an initial GO : BP ratio of 2:1. The enhanced performance is probably due to more efficient reduction of GO as the amount of reductive H_3PO_2 from the degradation of BP increases, this has been confirmed by the XPS characterization as the oxygen content of the as-derived RGO film decreased slightly from 16.21 at.% (GO:BP = 2:1) to 13.58 at.% (GO:BP = 1:2), see Figure S15 for the XPS survey and C1s spectra. In addition, the amount of acid electrolyte H_xPO_y

from BP degradation would also increase with higher content of BP in the initial hybrid film, thus prevent more RGO layers from compact restacking and allow fast ion movement inside the film.

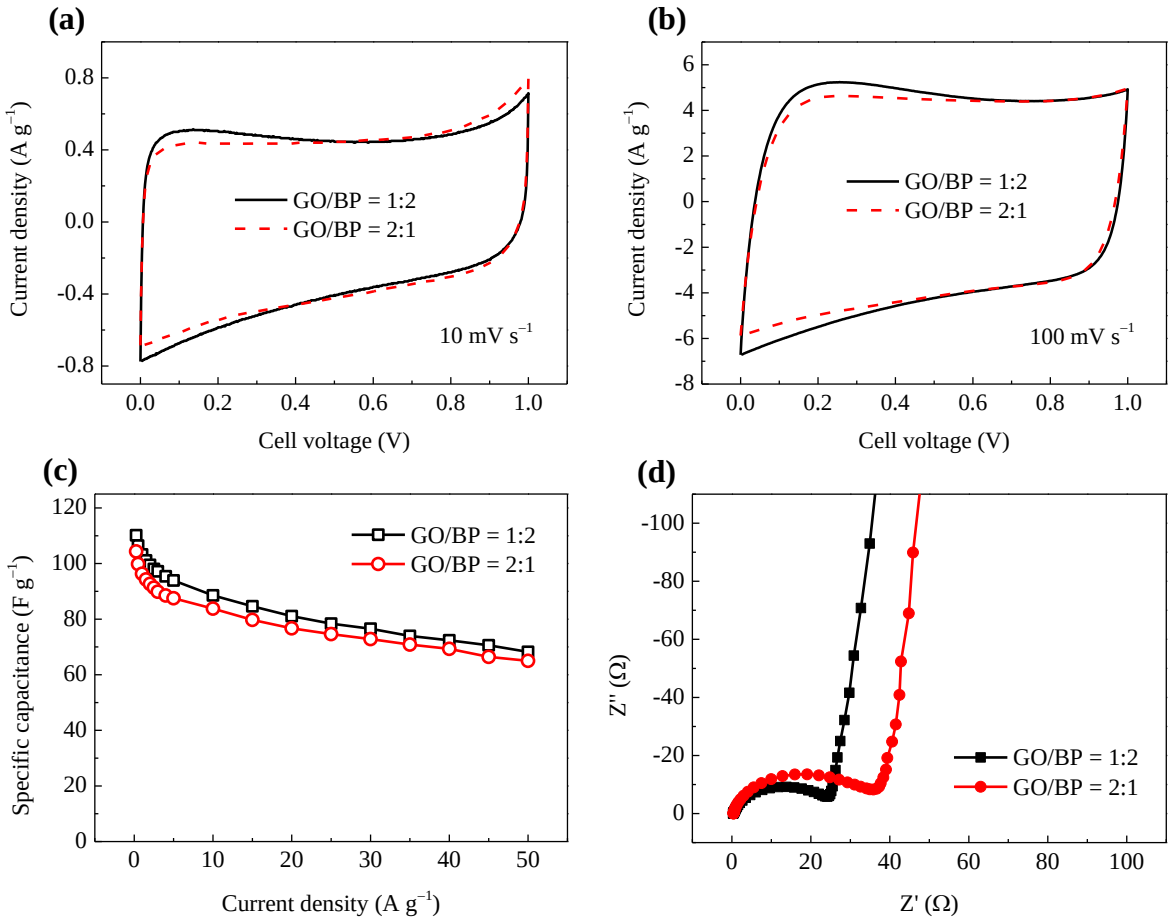

Figure 7. Electrochemical performances of supercapacitors based on RGO/H_xPO_y films derived from GO/BP films with different GO : BP mass ratio of 1:2 and 2:1. (a) and (b) comparison of CV curves at scan rates of 10 and 100 mV s^{-1}, respectively. (c) Evolution of specific capacitance with discharge current density. (d) Nyquist plots.

However, the enhancement in the electrochemical performance is not significant, as the specific capacitance just increased from 104 to 110 F g^{-1} by change the initial GO : BP ratio from 2:1 to 1:2. Taking the high cost of BP raw material and the low yield of few layers BP

by liquid phase exfoliation into consideration, the benefit from adding more BP into the initial GO/BP film is obviously not cost effective.

CONCLUSION

In summary, electrode materials with enhanced performance can be obtained from liquid phase exfoliated few-layer BP sandwiched between GO sheets after exposure to humid air. The oxidation of the BP leads to phosphorus acids (H_xPO_y) which reduce the GO to RGO and also act as a liquid electrolyte to prevent the compact restacking of the RGO sheets. The as-formed RGO/H_xPO_y film shows a high electrical conductivity of 837 ± 109 S m^{-1}. We propose that the presence of liquid H_xPO_y acids trapped between the RGO layers preserves inhibited channels for ion diffusion, leading to enhanced electrochemical performance. A supercapacitor based on the RGO/H_xPO_y film exhibits a specific capacitance of 104.4 F g^{-1} at 0.25 A g^{-1} and superior rate capability with 62.3% (65.0 F g^{-1}) of the initial capacitance retained at a high current density of 50 A g^{-1}, together with good cycling stability. The strategy of exploiting solid-liquid transformations to generate structural modification of film electrodes could lead to the development of high performance energy storage systems.

ASSOCIATED CONTENT

Supporting information

The supporting information is available free of charge on the ACS Publications website.

Experimental details; flake distribution of BP and GO flakes; AFM images and height profile of GO sheets; XRD pattern of BP crystal; XPS P2p core-level spectra of RGO/H_xPO_y and RGO film; EDX weight ratio of carbon (C), oxygen (O) and phosphorus (P) elements; Compare of FT-IR spectra of BP degradated products with that of H_3PO_2, H_3PO_3, and H_3PO_4;

XRD pattern of GO and GO films reduced by H_3PO_2, H_3PO_3 and H_3PO_4 at 50 °C for 12 h; CV curves at various scan rates, galvanostatic charging-discharging curves and Ragone plots of the supercapacitors based on RGO/H_xPO_y and RGO films, respectively; summay of BP degradation and GO reduciton under different enviroments and conditions; comparison of specific capacitance and cycling stabilty of various reported graphene based electrodes.

AUTHOR INFORMATION

Corresponding Authors

*pei.he@manchester.ac.uk

*brian.derby@manchester.ac.uk

Author contributions

The manuscript was written through contributions of all authors. All authors have given approval to the final version of the manuscript. ‡These authors contributed equally.

Notes

The authors declare no competing financial interest.

ACKNOWLEDGEMENTS

The authors are grateful to the Engineering and Physical Sciences Research Council (EPSRC), grant reference EP/N010345/1, EP/L012022/1, EP/K016954/1 and EP/L020742/1 for supporting this work.

REFERENCES

(1) Park, S.; Ruoff, R. S. Chemical methods for the production of graphenes. *Nat. Nanotechnol.* **2009,** *4* (4), 217-24.

(2) Dreyer, D. R.; Park, S.; Bielawski, C. W.; Ruoff, R. S. The chemistry of graphene oxide. *Chem. Soc. Rev.* **2010,** *39* (1), 228-40.

(3) Zhu, Y.; Murali, S.; Cai, W.; Li, X.; Suk, J. W.; Potts, J. R.; Ruoff, R. S. Graphene and graphene oxide: synthesis, properties, and applications. *Adv. Mater.* **2010,** *22* (35), 3906-24.

(4) Chua, C. K.; Pumera, M. Chemical reduction of graphene oxide: a synthetic chemistry viewpoint. *Chem. Soc. Rev.* **2014,** *43* (1), 291-312.

(5) Cao, J.; He, P.; Mohammed, M. A.; Zhao, X.; Young, R. J.; Derby, B.; Kinloch, I. A.; Dryfe, R. A. W. Two-Step Electrochemical Intercalation and Oxidation of Graphite for the Mass Production of Graphene Oxide. *J. Am. Chem. Soc.* **2017,** *139* (48), 17446-17456.

(6) Chen, H.; Müller, M. B.; Gilmore, K. J.; Wallace, G. G.; Li, D. Mechanically Strong, Electrically Conductive, and Biocompatible Graphene Paper. *Adv. Mater.* **2008,** *20* (18), 3557-3561.

(7) Li, D.; Muller, M. B.; Gilje, S.; Kaner, R. B.; Wallace, G. G. Processable aqueous dispersions of graphene nanosheets. *Nat Nanotechnol* **2008,** *3* (2), 101-5.

(8) Shao, Y.; El-Kady, M. F.; Wang, L. J.; Zhang, Q.; Li, Y.; Wang, H.; Mousavi, M. F.; Kaner, R. B. Graphene-based materials for flexible supercapacitors. *Chem. Soc. Rev.* **2015,** *44* (11), 3639-65.

(9) Wang, X.; Shi, G. Flexible graphene devices related to energy conversion and storage. *Energy Environ. Sci.* **2015,** *8* (3), 790-823.

(10) Yang, X.; Zhu, J.; Qiu, L.; Li, D. Bioinspired effective prevention of restacking in multilayered graphene films: towards the next generation of high-performance supercapacitors. *Adv. Mater.* **2011,** *23* (25), 2833-8.

(11) Yang, X.; Cheng, C.; Wang, Y.; Qiu, L.; Li, D. Liquid-mediated dense integration of graphene materials for compact capacitive energy storage. *Science* **2013,** *341* (6145), 534-7.

(12) Cheng, Y.; Lu, S.; Zhang, H.; Varanasi, C. V.; Liu, J. Synergistic effects from graphene and carbon nanotubes enable flexible and robust electrodes for high-performance supercapacitors. *Nano Lett.* **2012,** *12* (8), 4206-11.

(13) Wang, Y.; Chen, J.; Cao, J.; Liu, Y.; Zhou, Y.; Ouyang, J.-H.; Jia, D. Graphene/carbon black hybrid film for flexible and high rate performance supercapacitor. *J. Power Sources* **2014,** *271*, 269-277.

(14) Chen, J.; Wang, Y.; Cao, J.; Liu, Y.; Ouyang, J.-H.; Jia, D.; Zhou, Y. Flexible and solid-state asymmetric supercapacitor based on ternary graphene/MnO2/carbon black hybrid film with high power performance. *Electrochim. Acta* **2015,** *182*, 861-870.

(15) Brent, J. R.; Savjani, N.; Lewis, E. A.; Haigh, S. J.; Lewis, D. J.; O'Brien, P. Production of few-layer phosphorene by liquid exfoliation of black phosphorus. *Chem. Commun.* **2014,** *50* (87), 13338-41.

(16) Favron, A.; Gaufres, E.; Fossard, F.; Phaneuf-L'Heureux, A. L.; Tang, N. Y.; Levesque, P. L.; Loiseau, A.; Leonelli, R.; Francoeur, S.; Martel, R. Photooxidation and quantum confinement effects in exfoliated black phosphorus. *Nat. Mater.* **2015,** *14* (8), 826-32.

(17) Hanlon, D.; Backes, C.; Doherty, E.; Cucinotta, C. S.; Berner, N. C.; Boland, C.; Lee, K.; Harvey, A.; Lynch, P.; Gholamvand, Z.; Zhang, S.; Wang, K.; Moynihan, G.; Pokle, A.; Ramasse, Q. M.; McEvoy, N.; Blau, W. J.; Wang, J.; Abellan, G.; Hauke, F.; Hirsch, A.; Sanvito, S.; O'Regan, D. D.; Duesberg, G. S.; Nicolosi, V.; Coleman, J. N. Liquid exfoliation of solvent-stabilized few-layer black phosphorus for applications beyond electronics. *Nat. Commun.* **2015,** *6*, 8563.

(18) Del Rio Castillo, A. E.; Pellegrini, V.; Sun, H.; Buha, J.; Dinh, D. A.; Lago, E.; Ansaldo, A.; Capasso, A.; Manna, L.; Bonaccorso, F. Exfoliation of Few-Layer Black Phosphorus in

Low-Boiling-Point Solvents and Its Application in Li-Ion Batteries. *Chem. Mater.* **2018,** *30* (2), 506-516.

(19) Bat-Erdene, M.; Batmunkh, M.; Shearer, C. J.; Tawfik, S. A.; Ford, M. J.; Yu, L.; Sibley, A. J.; Slattery, A. D.; Quinton, J. S.; Gibson, C. T.; Shapter, J. G. Efficient and Fast Synthesis of Few-Layer Black Phosphorus via Microwave-Assisted Liquid-Phase Exfoliation. *Small Methods* **2017,** *1* (12), 1700260.

(20) Wood, J. D.; Wells, S. A.; Jariwala, D.; Chen, K. S.; Cho, E.; Sangwan, V. K.; Liu, X. L.; Lauhon, L. J.; Marks, T. J.; Hersam, M. C. Effective Passivation of Exfoliated Black Phosphorus Transistors against Ambient Degradation. *Nano Lett* **2014,** *14* (12), 6964-6970.

(21) Joshua, O. I.; Gary, A. S.; Herre, S. J. v. d. Z.; Andres, C.-G. Environmental instability of few-layer black phosphorus. *2D Materials* **2015,** *2* (1), 011002.

(22) Hanlon, D.; Backes, C.; Doherty, E.; Cucinotta, C. S.; Berner, N. C.; Boland, C.; Lee, K.; Harvey, A.; Lynch, P.; Gholamvand, Z.; Zhang, S.; Wang, K.; Moynihan, G.; Pokle, A.; Ramasse, Q. M.; McEvoy, N.; Blau, W. J.; Wang, J.; Abellan, G.; Hauke, F.; Hirsch, A.; Sanvito, S.; O'Regan, D. D.; Duesberg, G. S.; Nicolosi, V.; Coleman, J. N. Liquid exfoliation of solvent-stabilized few-layer black phosphorus for applications beyond electronics. *Nat Commun* **2015,** *6*, 8563.

(23) Brent, J. R.; Ganguli, A. K.; Kumar, V.; Lewis, D. J.; McNaughter, P. D.; O'Brien, P.; Sabherwal, P.; Tedstone, A. A. On the stability of surfactant-stabilised few-layer black phosphorus in aqueous media. *RSC Adv.* **2016,** *6* (90), 86955-86958.

(24) Huang, Y.; Qiao, J.; He, K.; Bliznakov, S.; Sutter, E.; Chen, X.; Luo, D.; Meng, F.; Su, D.; Decker, J.; Ji, W.; Ruoff, R. S.; Sutter, P. Interaction of Black Phosphorus with Oxygen and Water. *Chem. Mater.* **2016,** *28* (22), 8330-8339.

(25) Wang, Y.; Yang, B.; Wan, B.; Xi, X.; Zeng, Z.; Liu, E.; Wu, G.; Liu, Z.; Wang, W. Degradation of black phosphorus: a real-time31P NMR study. *2D Materials* **2016,** *3* (3), 035025.

(26) Zhou, Q.; Chen, Q.; Tong, Y.; Wang, J. Light-Induced Ambient Degradation of Few-Layer Black Phosphorus: Mechanism and Protection. *Angew. Chem. Int. Edit.* **2016,** *55* (38), 11437-41.

(27) Wang, X.; Xing, W.; Yu, B.; Feng, X.; Song, L.; Hu, Y. A facile and cost-effective approach to the reduction of exfoliated graphite oxide using sodium hypophosphite under acidic conditions. *J. Mater. Chem. C* **2013,** *1* (4), 690-694.

(28) Pei, H.; Brian, D. Inkjet printing ultra-large graphene oxide flakes. *2D Materials* **2017,** *4* (2), 021021.

(29) Cao, J. Y.; Wang, Y. M.; Chen, J. C.; Li, X. H.; Walsh, F. C.; Ouyang, J. H.; Jia, D. C.; Zhou, Y. Three-dimensional graphene oxide/polypyrrole composite electrodes fabricated by one-step electrodeposition for high performance supercapacitors. *J. Mater. Chem. A* **2015,** *3* (27), 14445-14457.

(30) Stoller, M. D.; Ruoff, R. S. Best practice methods for determining an electrode material's performance for ultracapacitors. *Energy Environ. Sci.* **2010,** *3* (9), 1294.

(31) Abraham, J.; Vasu, K. S.; Williams, C. D.; Gopinadhan, K.; Su, Y.; Cherian, C. T.; Dix, J.; Prestat, E.; Haigh, S. J.; Grigorieva, I. V.; Carbone, P.; Geim, A. K.; Nair, R. R. Tunable sieving of ions using graphene oxide membranes. *Nat Nanotechnol* **2017,** *12* (6), 546-550.

(32) Eigler, S. Controlled Chemistry Approach to the Oxo-Functionalization of Graphene. *Chem.-Eur. J.* **2016,** *22* (21), 7012-27.

(33) Hong, J. Y.; Kong, J.; Kim, S. H. Spatially controlled graphitization of reduced graphene oxide films via a green mechanical approach. *Small* **2014,** *10* (23), 4839-44.

(34) Hontorialucas, C.; Lopezpeinado, A. J.; Lopezgonzalez, J. D. D.; Rojascervantes, M. L.; Martinaranda, R. M. Study of oxygen-containing groups in a series of graphite oxides - physical and chemical characterisation. *Carbon* **1995,** *33* (11), 1585-1592.

(35) Withnall, R.; Andrews, L. FTIR spectra of the photolysis products of the phosphine ozone complex in solid argon. *J. Phys. Chem.* **1987,** *91* (4), 784-797.

(36) Kang, J.; Wells, S. A.; Wood, J. D.; Lee, J. H.; Liu, X. L.; Ryder, C. R.; Zhu, J.; Guest, J. R.; Husko, C. A.; Hersam, M. C. Stable aqueous dispersions of optically and electronically active phosphorene. *Proceedings of the National Academy of Sciences of the United States of America* **2016,** *113* (42), 11688-11693.

(37) Chen, W. F.; Yan, L. F.; Bangal, P. R. Chemical Reduction of Graphene Oxide to Graphene by Sulfur-Containing Compounds. *J. Phys. Chem. C* **2010,** *114* (47), 19885-19890.

(38) Zhou, X. J.; Zhang, J. L.; Wu, H. X.; Yang, H. J.; Zhang, J. Y.; Guo, S. W. Reducing Graphene Oxide via Hydroxylamine: A Simple and Efficient Route to Graphene. *J. Phys. Chem. C* **2011,** *115* (24), 11957-11961.

(39) Chen, C. M.; Zhang, Q.; Huang, C. H.; Zhao, X. C.; Zhang, B. S.; Kong, Q. Q.; Wang, M. Z.; Yang, Y. G.; Cai, R.; Sheng Su, D. Macroporous 'bubble' graphene film via template-directed ordered-assembly for high rate supercapacitors. *Chem. Commun.* **2012,** *48* (57), 7149-51.

(40) Parvez, K.; Wu, Z. S.; Li, R.; Liu, X.; Graf, R.; Feng, X.; Mullen, K. Exfoliation of graphite into graphene in aqueous solutions of inorganic salts. *J. Am. Chem. Soc.* **2014,** *136* (16), 6083-91.

(41) Liu, Y.; Li, Y.; Zhong, M.; Yang, Y.; Yuefang, W.; Wang, M. A green and ultrafast approach to the synthesis of scalable graphene nanosheets with Zn powder for electrochemical energy storage. *J. Mater. Chem.* **2011,** *21* (39), 15449.

(42) Wang, S.; Dryfe, R. A. W. Graphene oxide-assisted deposition of carbon nanotubes on carbon cloth as advanced binder-free electrodes for flexible supercapacitors. *J. Mater. Chem. A* **2013,** *1* (17), 5279.

(43) Weng, Z.; Su, Y.; Wang, D.-W.; Li, F.; Du, J.; Cheng, H.-M. Graphene-Cellulose Paper Flexible Supercapacitors. *Adv. Energy Mater.* **2011,** *1* (5), 917-922.

(44) Lin, Y.; Liu, F.; Casano, G.; Bhavsar, R.; Kinloch, I. A.; Derby, B. Pristine Graphene Aerogels by Room-Temperature Freeze Gelation. *Adv. Mater.* **2016,** *28* (36), 7993-8000.

For Table of Contents Only